Eur. Phys. J. B **41**, 457–470 (2004)
DOI: 10.1140/epjb/e2004-00339-x

THE EUROPEAN PHYSICAL JOURNAL B

Aging, rejuvenation, and memory effects in short-range Ising spin glass: $Cu_{0.5}Co_{0.5}Cl_2$-$FeCl_3$ graphite bi-intercalation compound

M. Suzuki[a] and I.S. Suzuki

Department of Physics, State University of New York at Binghamton, Binghamton, New York 13902-6000, USA

Received 31 July 2003 / Received in final form 13 September 2004
Published online 5 November 2004 –

Abstract. Non-equilibrium aging dynamics in 3D Ising spin glass $Cu_{0.5}Co_{0.5}Cl_2$-$FeCl_3$ GBIC has been studied by zero-field cooled (ZFC) magnetization and low frequency AC magnetic susceptibility ($f = 0.05$ Hz), where $T_g = 3.92 \pm 0.11$ K. The time dependence of the relaxation rate $S(t) = (1/H)\mathrm{d}M_{\mathrm{ZFC}}/\mathrm{dln}\, t$ for the ZFC magnetization after the ZFC aging protocol, shows a peak at a characteristic time t_{cr} near a wait time t_w (aging behavior), corresponding to a crossover from quasi equilibrium dynamics to non-equilibrium. The time t_{cr} strongly depends on t_w, temperature (T), magnetic field (H), and the temperature shift (ΔT). The rejuvenation effect is observed in both χ' and χ'' under the T-shift and H-shift procedures. The memory of the specific spin configurations imprinted during the ZFC aging protocol can be recalled when the system is re-heated at a constant heating rate. The aging, rejuvenation, and memory effects observed in the present system are discussed in terms of the scaling concepts derived from numerical studies on 3D Edwards-Anderson spin glass model.

PACS. 75.50.Lk Spin glasses and other random magnets – 75.10.Nr Spin-glass and other random models – 75.40.Gb Dynamic properties

1 Introduction

In recent years, non-equilibrium dynamics, in particular, aging dynamics, of spin glass (SG) systems has been extensively studied theoretically [1–9] and experimentally [10–28]. When the SG system is quenched from a high temperature above the SG transition temperature T_g to a low temperature T below T_g (this process is called the zero-field cooled (ZFC) aging protocol), the initial state is not thermodynamically stable and relaxes to more stable state. The aging behaviors depend strongly on their thermal history within the SG phase. A typical experimental method for the study of the aging dynamics is the time dependence of the ZFC magnetization (M_{ZFC}) after the ZFC aging protocol. When a small magnetic field (H) is applied after an isothermal aging at a temperature T below T_g for a wait time t_w, M_{ZFC} increases as an observed time (t) increases. The rejuvenation (chaos) and memory effects are also significant features of the aging dynamics. These effects are typically measured from the low frequency AC magnetic susceptibility.

Such an aging dynamics of SG phase is explained mainly in terms of a real-space picture (the droplet model) [1]. In this picture, the SG coherence length for equilibrium SG order, grows up slowly in aging processes. The scaling properties of age-dependent macroscopic susceptibility can be described by a growing coherence length $L_T(t)$. The droplet model also predicts the following two. (i) The equilibrium SG states at two temperatures with the difference ΔT are uncorrelated in length scales larger than the overlap length $L_{\Delta T}$, i.e., so-called temperature (T)-chaos nature of the SG phase. (ii) In the equilibrium and thermodynamic limits the SG phase is broken by a static magnetic field H of infinitesimal strength, thereby introduced is the crossover length L_H. This length separates the mean size of SG domains $L_T(t)$, such that they are dominated by the Zeemann energy for $L_T(t) > L_H$ and by the SG free energy gap for $L_T(t) \ll L_H$. Recently Monte Carlo (MC) simulations [7,8] on the T- and H-shift aging processes have been carried out for the three-dimensional (3D) Ising Edwards-Anderson (EA) SG model with Gaussian nearest-neighbor interactions with zero mean and variance J, where J is in the unit of energy. In the T-shift process, only a precursor of the temperature-chaos effect is observed, while the results on the H-shift process strongly support the droplet picture that the SG phase under a finite H is unstable in the equilibrium and thermodynamic limits.

In this paper we report our results on the aging dynamics (aging, rejuvenation and memory) of a 3D Ising SG, $Cu_{0.5}Co_{0.5}Cl_2$-$FeCl_3$ graphite bi-intercalation compound (GBIC). The aging behavior of the ZFC magnetization has been measured at various aging processes including the T- and H-shift perturbations. The rejuvenation effect of the low frequency AC magnetic susceptibility has been measured at aging processes including

[a] e-mail: suzuki@binghamton.edu

the T- and H-shift perturbations. The memory of the specific spin configurations imprinted during the ZFC aging protocol can be recalled when the system is re-heated at a constant heating rate. The existence of the characteristic lengths $L_{\Delta T}$ and L_H is examined by the T- and H-shift aging protocols. The relaxation rate defined by $S(t) = (1/H)\mathrm{d}M_{\mathrm{ZFC}}/\mathrm{dln}\,t$ (see Sect. 2.2 for more definitions) exhibits a peak at a characteristic time t_{cr}, which is comparable to a wait time t_w. We show that the ratio t_{cr}/t_w strongly depends on the aging process. These results are compared with those reported for typical spin glass systems such as Cu (1.5–13.5 at.% Mn) [12–15,22,23,25,27], Ag (11 at.% Mn) [16,21,28], $CdCr_{1.7}In_{0.3}S_4$ [17,18], $Fe_{0.5}Mn_{0.5}TiO_3$ [5,19,20], as well as results from MC simulations [2,4,7,8].

The equilibrium dynamics of $Cu_{0.5}Co_{0.5}Cl_2$-$FeCl_3$ GBIC has been reported in a previous paper [26]. The aging dynamics has been also studied: the ωt-scaling of χ' and χ'' is also confirmed, where ω is the angular frequency of the AC magnetic field. This compound undergoes a SG transition at T_g ($= 3.92 \pm 0.11$ K). The system shows a dynamic behavior that has some similarities and some significant differences compared to a 3D Ising SG. It shows critical slowing down with a value of the dynamic critical exponent that is rather similar to an Ising SG: $z = 6.6 \pm 1.2$, $\theta = 0.13 \pm 0.02$, and $\psi = 0.24 \pm 0.02$, where z, ψ, and θ are the dynamic critical exponent, the stiffness exponent (energy exponent) which determines the free energy of a droplet excitation, and the barrier exponent which describes how the barrier heights change with length scale. The critical relaxation time τ is well described by $\tau = \tau^*(1 - T/T_g)^{-x}$ with the dynamic critical exponent $x = 10.3 \pm 0.7$ and $\tau^* = (5.29 \pm 0.07) \times 10^{-6}$ s. The in-field dynamics indicates, as for an Ising SG, that the SG transition is destroyed by a magnetic field. The equilibrium dynamics shows a frequency dependence that is different from an Ising SG, the absorption decreases with increasing frequency, whereas ordinary 3D Ising SG shows a increasing absorption with increasing frequency. An aging behavior is observed that is rejuvenated by a large enough (magnetic field) perturbation.

2 Background

2.1 Scaling properties

We present a simple review on the aging behavior of SG phase after the ZFC aging protocol, based on the droplet model [1,2,10]. This ZFC aging protocol process to the SG phase is completed at $t_a = 0$, where t_a is defined as an age (the total time after the ZFC aging protocol process). Then the system is aged at T under $H = 0$ until $t_a = t_w$, where t_w is a wait time. Correspondingly, the size of domain defined by $R_T(t_a)$ grows with the age of t_a and reaches $R_T(t_w)$ just before the field is turned on at $t = 0$ or $t_a = t_w$. The aging behavior in M_{ZFC} is observed as a function of the observation time t. After $t = 0$, a probing length $L_T(t)$ corresponding to the maximum size of excitation grows with t, in a similar way as $R_T(t_a)$. When $L_T(t) \ll R_T(t_w)$, quasi-equilibrium dynamics is probed, but when $L_T(t) \gg R_T(t_w)$, non-equilibrium dynamics is probed. It is theoretically predicted that the mean SG domain-size $L_T(T)$ is described by a power law given by [2]

$$L_T(t)/L_0 \approx (t/t_0)^{1/z(T)}, \tag{1}$$

or by [1]

$$L_T(t)/L_0 \approx [(T/\Delta_g)\ln(t/t_0)]^{1/\psi}, \tag{2}$$

where L_0 and t_0 are microscopic length and time scale, the exponent $1/z(T)$ ($= bT/T_g$ with $b = 0.16$) [2] linearly depends on T except for the region near T_g, and Δ_g and ψ are the characteristic scale of energy barrier of droplet excitations and the associated exponent, respectively. It is predicted by Komori et al. [2] that $\Delta\chi''$ obeys the ωt-scaling form given by $\Delta\chi'' \approx (\omega t)^{-b''}$ where $b'' = (d - \theta)/z(T)$, d ($= 3$) is the dimension, and $\theta = 0.20 \pm 0.03$. Experimentally, as shown in our previous paper [26], $\Delta\chi''(\omega, t)$ at 3.75 K obeys the ωt-scaling law, $\Delta\chi''(\omega, t) \approx (\omega t)^{-b''}$ with $b'' = 0.255 \pm 0.005$, where $\Delta\chi''(\omega, t) = \chi''(\omega, t) - \langle\chi_0''(\omega)\rangle$, where $\langle\chi_0''(\omega)\rangle$ is the stationary frequency-dependent absorption.

2.2 S(t) and $\chi''(t_w; t + t_w)$

Here we present a simple review on the relation between $S(t)$ and χ''. The absorption χ'' is evaluated from the spin auto-correlation function $C(t_a - t; t_a) = \overline{\langle S_i(t_a - t)S_i(t_a)\rangle}$ using the fluctuation-dissipation theorem (FDT) as [2,7]

$$\chi''(\Delta t_\omega; t + \Delta t_\omega) \approx (-\pi/2T)\partial C(\Delta t_\omega; t + \Delta t_\omega)/\partial \ln t, \tag{3}$$

where $t_a = t + \Delta t_\omega$, $\Delta t_\omega = 2\pi/\omega$ (typically $\Delta t_\omega \leq 10^2$ s) and t is much larger than Δt_ω. In the auto-correlation function, the over-line denotes the average over sites and over different realizations of bond disorder, and the bracket the average over thermal noises. For slow processes, the dispersion $\chi'(\Delta t_\omega; t + \Delta t_\omega)$ is approximated by

$$\chi'(\Delta t_\omega; t + \Delta t_\omega) \approx [1 - C(\Delta t_\omega; t + \Delta t_\omega)]/T. \tag{4}$$

In the quasi-equilibrium regime where the FDT holds, the ZFC susceptibility $\chi_{\mathrm{ZFC}}(t_w;\ t{+}t_w)$ is described by [2,4]

$$\chi_{\mathrm{ZFC}}(t_w; t + t_w) \approx [1 - C(t_w; t + t_w)]/T, \tag{5}$$

where $t_a = t + t_w$ and t_w is a wait time: typically, $t_w \approx 10^3$–10^5 s. Then the relaxation rate $S(t)$ is described by

$$\begin{aligned} S(t) &= \mathrm{d}\chi_{\mathrm{ZFC}}(t_w; t + t_w)\mathrm{d}\ln t \\ &= (-1/T)\partial C(t_w; t + t_w)/\partial \ln t, \end{aligned} \tag{6}$$

which corresponds to $(2/\pi)\chi''(t_w; t + t_w)$ [10].

It is predicted that $C(t_w; t + t_w)$ can be decomposed into a stationary part $C_{st}(t)$ and an aging part $C_{ag}(t_w; t + t_w)$ [6]. The latter is approximately described by a scaling function of $L_T(t)$ and $R_T(t_w)$. The corresponding aging part of $S(t)$ exhibits a peak at a characteristic time t_{cr} ($\approx t_w$) [6,29], where $L_T(t) \approx R_T(t_w)$, showing a crossover between quasi-equilibrium region and non-equilibrium region.

3 Experimental procedure

The DC magnetization and AC susceptibility of $Cu_{0.5}Co_{0.5}Cl_2$-$FeCl_3$ GBIC were measured using a SQUID magnetometer (Quantum Design, MPMS XL-5) with an ultra low field capability option. The remnant magnetic field was reduced to zero field (exactly less than 3 mOe) at 298 K for both DC magnetization and AC susceptibility measurements. The AC magnetic field used in the present experiment has a peak magnitude of $h = 0.1$ Oe and frequency $f = \omega/2\pi = 0.05$ Hz. Each experimental procedure for measurements is presented in the text and figure captions. The detail of sample characterizations and sample preparation is given in the previous paper [26].

In our measurement of the time (t) dependence of the zero-field cooled (ZFC) magnetization ($M_{\rm ZFC}$), the time required for the ZFC aging protocol and subsequent wait time was precisely controlled. Typically it takes 240 ± 3 s to cool the system from 10 K to 3.75 K. It takes another $t_{w0} = 230 \pm 3$ s until T (= 3.75 K) becomes stable within the uncertainty (±0.01 K). The system is kept at $T = 3.75$ K and $H = 0$ for a wait time t_w ($0 \leq t \leq 3 \times 10^4$ s). The time for setting up a magnetic field from $H = 0$ to $H = 5$ Oe is 68 ± 2 s. In the ZFC measurement, the sample is slowly moved through the pick-up coils over the scan length (4 cm). The magnetic moment of the sample induces a magnetic flux change in the pick-up coils. It takes 12 s for each scan. The data at t is regarded as the average of $M_{\rm ZFC}$ measured over the scanning time t_s between the times $t-(t_s/2)$ and $t-(t_s/2)$. Thus the time window Δt is a scanning time (t_s). The measurement was carried out at every interval of $t_s + t_p$, where t_p is a pause between consecutive measurements. Typically we used (i) the time window $\Delta t = 36$ s for three scans and $t_p = 45$ s or 30 s for t_w ($\geq 2.0 \times 10^3$ s), and (ii) the time window $\Delta t = 12$ s for one scan and $t_p = 1$ or 2 s for either t_w ($\leq 10^3$ s) or $H \geq 100$ Oe.

4 Result

4.1 S(t) : t_w and T dependence

The t dependence of $M_{\rm ZFC}$ was measured under various conditions. Figure 1a shows the T dependence of the ZFC and FC magnetization ($M_{\rm ZFC}$ and $M_{\rm FC}$) at $H = 5$ Oe, where H is applied along a direction perpendicular to the c axis. The system was quenched from 50 to 1.9 K in the absence of H before the measurement. The change of T with the time t during the measurement is shown in Figure 1b. The ZFC magnetization was measured with increasing T from 1.9 to 3.75 K in the presence of H (= 5 Oe). The system was kept at $T = 3.75$ K for 2.27×10^4 s. Subsequently the ZFC measurement was continued from 3.75 to 8 K. The system was annealed at 50 K for 1.2×10^3 s. The FC magnetization was measured from 8 to 1.9 K. There is a remarkable increase of $M_{\rm ZFC}$ during the one stop at $T = 3.75$ K. When the warming up of the system was restarted, the increase in $M_{\rm ZFC}$ with T is much weaker than that in $M_{\rm ZFC}^{ref}$ as a reference without the stop: $M_{\rm ZFC}$ merges with $M_{\rm ZFC}^{ref}$ well above T_g. Similar result of $M_{\rm ZFC}$ vs. T was reported for a 3D Ising SG $Fe_{0.5}Mn_{0.5}TiO_3$. Bernardi et al. [5] have concluded that $M_{\rm ZFC}$ is described by a scaling function of $R_T(t_w)$ and $L_T(t)$ [$M_{\rm ZFC}(T,t) = G(L_T(t), R_T(t_w))$], where G is the scaling function. The t dependence of $M_{\rm ZFC}$ was monitored during the stop at $T = 3.75$ K, where the time taken during the measurement from 1.9 to 3.75 K was 5.4×10^3 s, corresponding to a wait time t_w. Figure 1c shows the t dependence of the relaxation rate $S(t)$, where the origin of t ($t = 0$) is a time when T reaches 3.75 K.

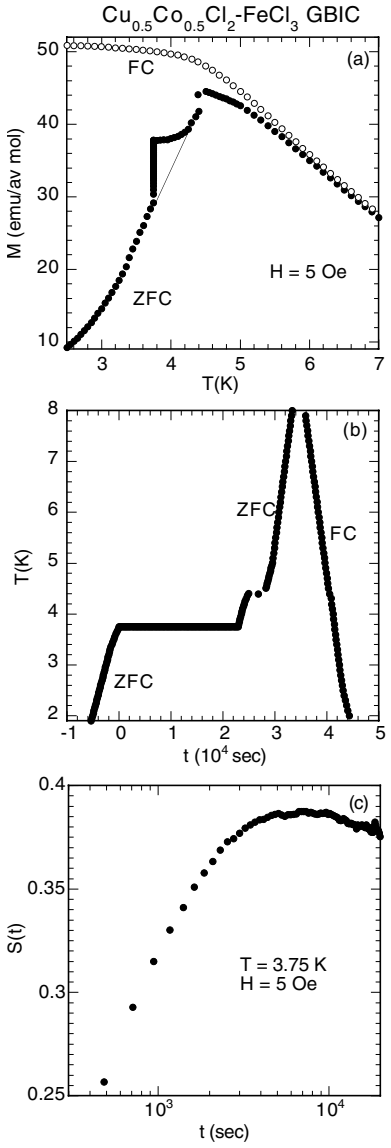

Fig. 1. (a) T dependence of $M_{\rm ZFC}$ and $M_{\rm FC}$ at $H = 5$ Oe for $Cu_{0.5}Co_{0.5}Cl_2$-$FeCl_3$ GBIC. The measurement was carried out after the ZFC aging protocol: annealing of the system at 50 K for 1.2×10^3 s at $H = 0$ and quenching from 50 to 1.9 K. During the ZFC measurement the system was aging at 3.75 K for 2.27×10^4 s. (b) The change of T with t during the measurement of $M_{\rm ZFC}$ and $M_{\rm FC}$. The discontinuity of T with t at $T = 4.4$ K is due to the system error occurring in the process of temperature stabilization. (c) The relaxation rate $S(t)$ (= $(1/H)\mathrm{d}M_{\rm ZFC}(t)/\mathrm{d}\ln t$) at 3.75 K. The time taken during the measurement of $M_{\rm ZFC}$ from 1.9 to 3.75 K at $H = 5$ Oe was $t_0 = 5.4 \times 10^3$ s. $t = 0$ is a time just after T becomes 3.75 K.

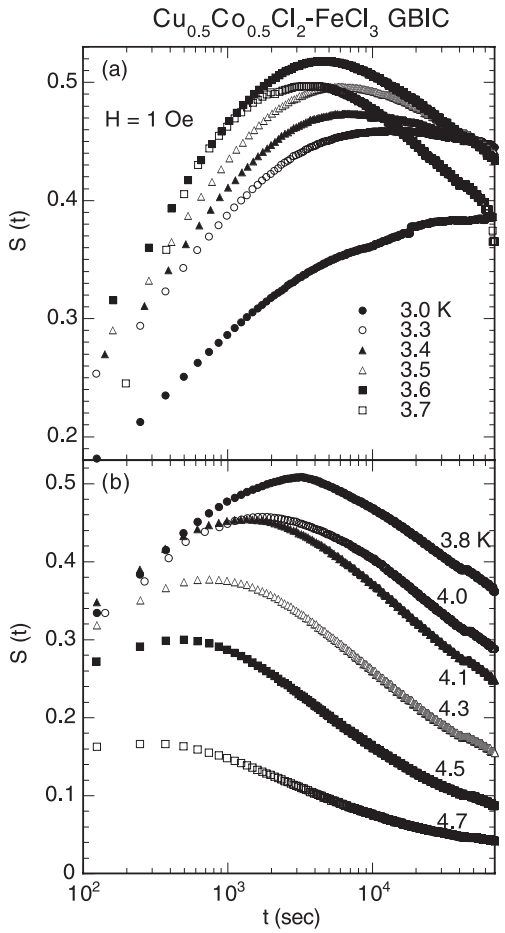

Fig. 2. (a) and (b) t dependence of S for $3.0 \leq T \leq 4.7$ K. $H = 1$ Oe. The measurement of $\chi_{\rm ZFC}$ vs. t was carried out after the ZFC aging protocol (annealing of the system at 50 K and $H = 0$ for 1.2×10^3 s, quenching from 50 K to T, and isothermal aging for $t_w = 2.0 \times 10^3$ s). $t = 0$ is the time just after $H = 1$ Oe is applied at T.

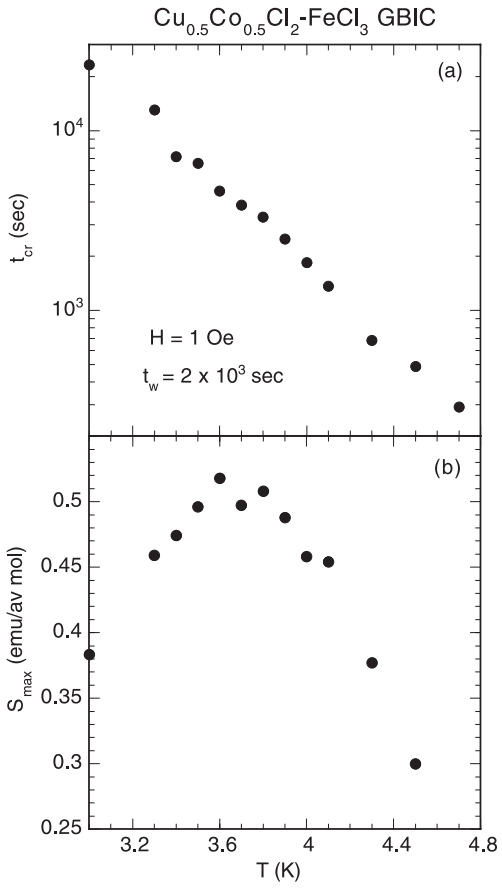

Fig. 3. T dependence of t_{cr} at which $S(t)$ has a peak value S_{max}. $t_w = 2.0 \times 10^3$ s. $H = 1$ Oe. (b) T dependence of the peak height S_{max} (see Fig. 2).

We have measured the t dependence of $\chi_{\rm ZFC}$ ($= M_{\rm ZFC}/H$) at various fixed T, where $t_w = 2.0 \times 10^3$ s and $H = 1$ Oe. The measurement was carried out after the ZFC aging protocol: annealing of the system at $T = 50$ K and $H = 0$ for 1.2×10^3 s, quenching from 50 K to T at $H = 0$, and isothermal aging at T for t_w. The origin of t ($t = 0$) is a time just after $H = 1$ Oe is applied at T. We find that $M_{\rm ZFC}$ increases with increasing t, depending on T. Figures 2a and b show the t dependence of S at various T ($3.0 \leq T \leq 4.7$ K), where $H = 1$ Oe and $t_w = 2.0 \times 10^3$ s. Each $S(t)$ curve exhibits a peak at a characteristic time t_{cr}, shifting to the short t-side with increasing T. The peak width becomes much broader with decreasing T. Figures 3a and b show the T dependence of t_{cr} and the peak height S_{max}, respectively, which are derived from Figures 2a and b. The characteristic time t_{cr} increases with decreasing T. The T dependence of $\ln(t_{cr}/t_w)$ will be discussed in Section 5 in association with the scaling relations. The peak height S_{max} exhibits a broad peak between 3.6 and 3.8 K just below T_g. Similar behavior of S vs. t at various T ($< T_g$) has been reported by Zotev et al. for Cu (1.5 at.% Mn) [23], where $S(t)$ is defined from the thermoremnant magnetization $M_{\rm TR}$ instead of $M_{\rm ZFC}$. The relaxation rate $S(t)$ exhibits a peak at $t = t_{cr}$, whose peak width becomes much broader with decreasing T. The peak height S_{max} decreases with decreasing T below T_g.

Figure 4a shows the t dependence of S at various t_w, where $T = 3.75$ K and $H = 5$ Oe. The relaxation rate $S(t)$ shows a peak at $t = t_{cr}$, shifting to the long-t side with increasing t_w. Similar behavior of $S(t)$ vs. t at various t_w has been observed by Jönsson et al. for Ag (11 at.% Mn) [21], where $t_{cr} \approx t_w$. In Figure 4b we show the characteristic time t_{cr} as a function of t_w for $0 \leq t_w \leq 3.0 \times 10^4$ s, where a straight line denotes the relation described by $t_{cr} = (0.68 \pm 0.03) t_w$. Figure 4c shows the plot of $S(t)/S_{max}$ as a function of t/t_w, where only the data of S vs. t with long t_w ($5 \times 10^3 \leq t_w \leq 1.5 \times 10^4$ s) for $0 < t < 6 \times 10^4$ s are used. It seems that $S(t)/S_{max}$ is well described by a scaling function of t/t_w [$S(t)/S_{max} = F(t/t_w)$] in the region of long t_w, although the data at $t_w = 1.5 \times 10^4$ s slightly deviates from the other data. The scaling function $F(x)$ has a very broad peak centered at $x \approx 0.68$. This result suggests that the spin auto-correlation function $C(t_w, t + t_w)$ is described by a scaling function of only t/t_w, since it is related to $S(t)$ by equation (6).

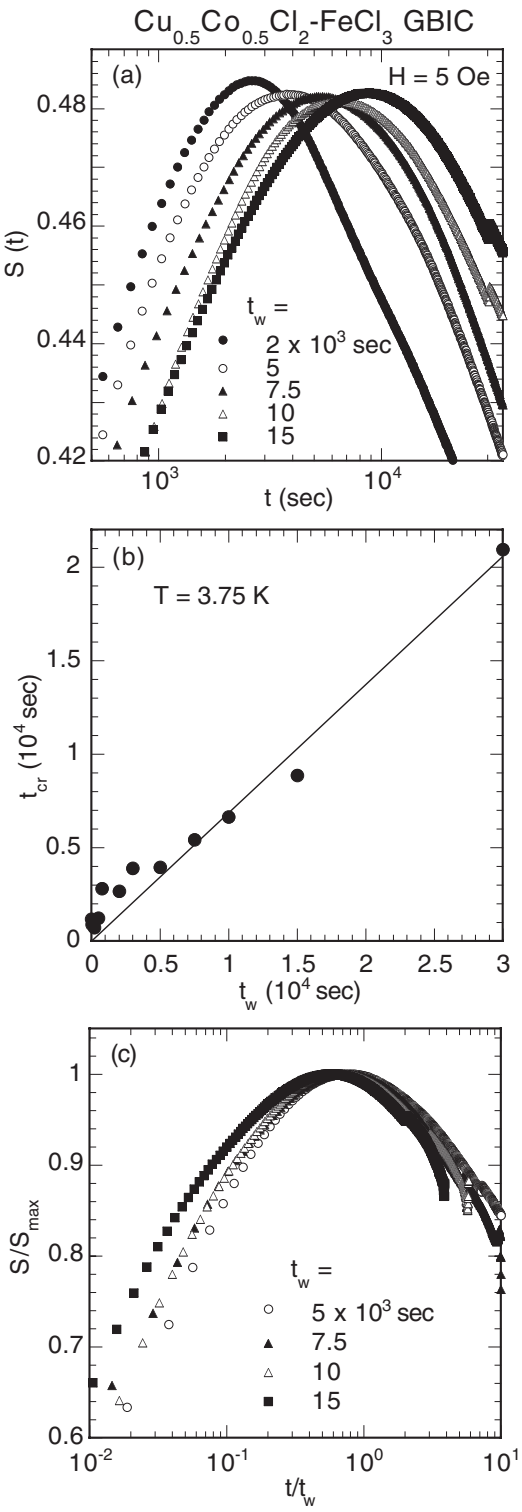

Fig. 4. (a) t dependence of S for $0 \leq t_w \leq 1.5 \times 10^4$ s. $T = 3.75$ K. $H = 5$ Oe. The ZFC aging protocol: annealing of the system at 50 K for 1.2×10^3 s at $H = 0$, quenching from 50 to 3.75 K, and then isothermal aging at 3.75 K and $H = 0$ for a wait time t_w. The measurement was started at $t = 0$ when the field H is turned on. (b) t_{cr} vs. t_w. The straight line denotes a relation given by $t_{cr} = (0.68 \pm 0.03)t_w$. (c) Scaling plot of S/S_{max} vs. t/t_w for the limited t_w and t ($5.0 \times 10^3 \leq t_w \leq 1.5 \times 10^4$ s, $0 \leq t \leq 6.0 \times 10^4$ s).

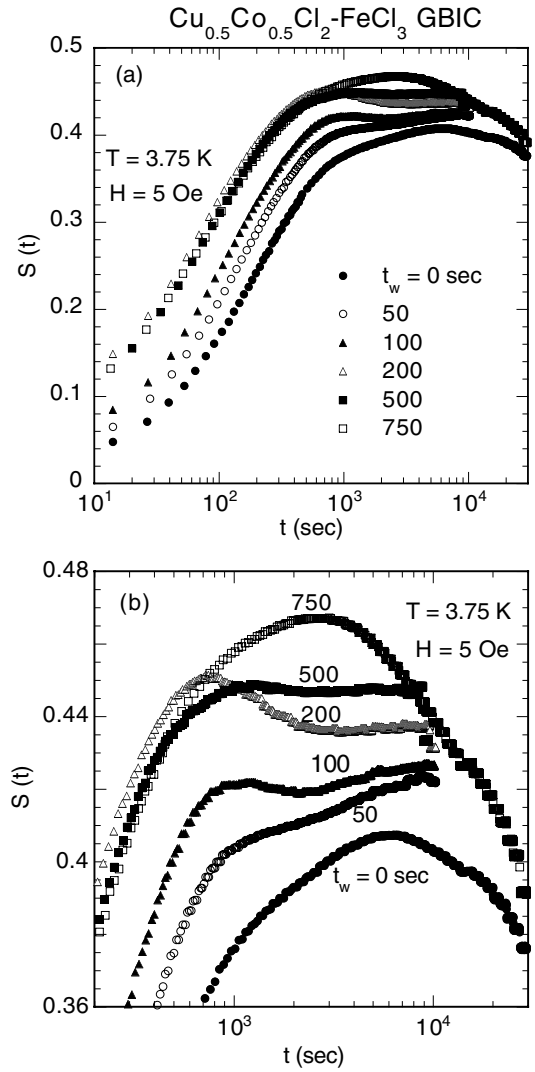

Fig. 5. (a) and (b) t dependence of S for $0 \leq t_w \leq 750$ s. $T = 3.75$ K. $H = 5$ Oe.

4.2 S(t) for $0 \leq t_w \leq 750$ s

We have measured the t dependence of $\chi_{\rm ZFC}$ at $T = 3.75$ K and $H = 5$ Oe as a wait time t_w ($0 \leq t_w \leq 750$ s) is varied as a parameter. The measurement was carried out after the ZFC aging protocol: annealing of the system at 50 K for 1.2×10^3 s at $H = 0$, quenching from 50 to 3.75 K, and then isothermal aging at $T = 3.75$ K and $H = 0$ for a wait time t_w. The origin of t ($t = 0$) is a time just after the field H is turned on. As is described in Section 3, it takes $t_{w0} = 230 \pm 3$ s until the temperature becomes stable at 3.75 K within the experimental uncertainty of ± 0.01 K, after quenching the system from 50 to 3.75 K at $H = 0$. This time t_{w0} is not included in the wait time t_w. If t_{w0} is included in t_w, however, the effective wait time may be longer than t_w^{eff} ($= t_{w0} + t_w$). If this is the case, the measurement with $t_w = 0$ is not possible in a strict sense. In spite of such a situation, here we assume that t_0 is not included in t_w. Figures 5a and b show the t dependence of S for $0 \leq t_w \leq 750$ s, where $T = 3.75$ K and $H = 5$ Oe.

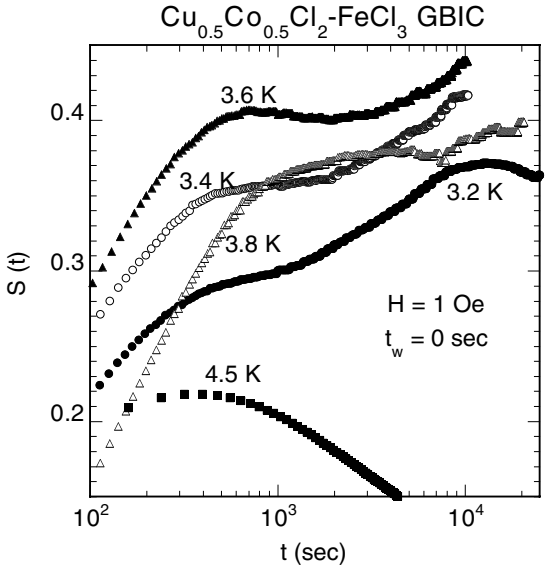

Fig. 6. t dependence of S at various T. $t_w = 0$ s. $H = 1$ Oe.

For $t_w = 0$, $S(t)$ shows a shoulder around $t = 10^3$ s and a broad peak at $t_{cr} = 6.45 \times 10^3$ s. For $t_w = 100$ s, a small peak of $S(t)$ is observed at $t_{cr} = 1.06 \times 10^3$ s in addition to a possible broad peak around $t_{cr} = 1.0 \times 10^4$ s. This small peak shifts to the short t-side with increasing t_w: $t_{cr} = 740$ s for $t_w = 200$ s. For $t_w = 750$ s, a broad peak is observed at $t_{cr} = 2.8 \times 10^3$ s. The values of t_{cr} thus obtained are also plotted as a function of t_w in Figure 4b. It should be noted that that for very short t_w ($0 \leq t \leq 200$ s), there are at least two kinds of domains: domains with large size corresponding to long t_{cr} ($\approx 6.5 \times 10^3$ s) coexist with domains with small size corresponding to short t_{cr} (≈ 750 s) in the regular aging regime. Figure 6 shows the t dependence of $S(t)$ at various T ($3.4 \leq T \leq 4.5$ K) and $H = 1$ Oe for $t_w = 0$. At $T = 3.2$ K, $S(t)$ shows a shoulder around $t = 400$ s and a very broad peak at $t_{cr} = 7.1 \times 10^3$ s. This shoulder shifts to the long t-side with increasing T and changes in to a broad peak. At $T = 3.6$ K, $S(t)$ shows a peak at $t_{cr} = 710$ s. It tends to increase with further increasing t, suggesting that t_{cr} is longer than 10^4 s. At $T = 3.8$ K, $S(t)$ shows a very broad peak centered at $t_{cr} = 3.8 \times 10^3$ s.

Similar behavior has been reported by Rodriguez et al. [25] in the time decay of the thermal remnant magnetization (TRM) of $Cu_{0.94}Mn_{0.06}$ ($T_g = 31.5$ K) with various wait time ($t_w = 0$–10^4 s) and a series of rapid FC cooling protocol from 35 to 26 K at H (= 20 Oe). The relaxation rate $S(t)[= -(1/H)\mathrm{d}M_{\mathrm{TRM}}(t)/\mathrm{dln}\,t]$ for $M_{\mathrm{TRM}}(t)$ is equivalent to $S(t)$ $[= -(1/H)\mathrm{d}M_{\mathrm{ZFC}}(t)/\mathrm{dln}\,t]$ for $M_{\mathrm{ZFC}}(t)$. They have shown that $S(t)$ at $t_w = 0$ exhibits a broad peak at an effective time t_c^{eff} (= 19–406 s), which is strongly dependent on the FC cooling protocol. For the larger t_c^{eff}, there is a significant contamination in $S(t)$ at t_w ($\neq 0$) from the FC cooling protocol. Recently the long-time decay of $M_{\mathrm{TRM}}(t)$ has been also examined by Kenning et al. [27] for the same system with rapid FC cooling protocol and short wait time ($t_w = 7$–110 s).

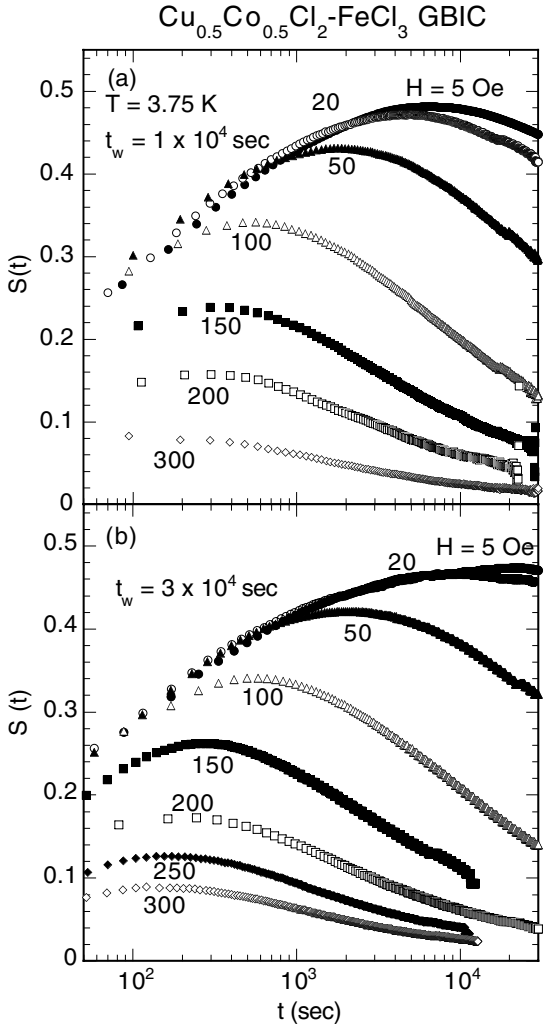

Fig. 7. t dependence of S for $5 \leq H \leq 300$ Oe. $T = 3.75$ K. (a) $t_w = 1.0 \times 10^4$ s. (b) $t_w = 3.0 \times 10^4$ s. The time $t = 0$ is a time when H is turned on. The ZFC aging protocol before the measurement is similar to that used in Figure 2.

A t_w-independent long-time decay overlaps with the t_w-dependent short-time decay. For the short-time decay, the corresponding $S(t)$ exhibits a peak at t_{cr} ($\approx t_w$). The long-time decay may be related to the initial state distribution developed during the FC cooling protocol.

4.3 S(t) under the H-shift

We have measured the t dependence of χ_{ZFC} at $T = 3.75$ K for various H, where $t_w = 1.0 \times 10^4$ and 3.0×10^4 s. The measurements were carried out after the ZFC aging protocol: annealing of the system at $T = 50$ K and $H = 0$ for 1.2×10^3 s, quenching from 50 to 3.75 K at $H = 0$, and isothermal aging at 3.75 K for t_w. The origin of t ($t = 0$) is the time just after H is turned on. The window time used in this measurement was 12 s. Figures 7a and b show the t dependence of S for $t_w = 1.0 \times 10^4$ s and 3.0×10^4 s as H is varied as a parameter, where $T = 3.75$ K. The relaxation rate $S(t)$ exhibits a peak

at $t = t_{cr}$, corresponding to a characteristic time scale of crossover from the isothermal aging state under $H = 0$ to that under a finite H. Figure 8a shows the plot of t_{cr} at $T = 3.75$ K as a function of H for $t_w = 1.0 \times 10^4$ and 3.0×10^4 s. The value of t_{cr} for $t_w = 1.0 \times 10^4$ and 3.0×10^4 s drastically decreases with increasing H. The value of t_{cr} for $t_w = 3 \times 10^4$ s is much larger than that for $t_w = 1 \times 10^4$ s at low H ($H < 50$ Oe). However, they are almost identical irrespective of t_w for high H ($H > 100$ Oe). We note that $\ln t_{cr}$ is linearly dependent on H only for $H < H_\alpha$: $H_\alpha \approx 50$ Oe for $t_w = 3.0 \times 10^4$ s and 100 Oe for $t_w = 1.0 \times 10^4$ s. In Figure 8b we show the H dependence of S_{max}. The peak value S_{max} linearly decreases with increasing H irrespective of t_w and tends to reduce to zero above 300 Oe. Similar behavior of t_{cr} vs. H has been reported by Zotev et al. [22] in Cu (1.5 at.% Mn). The break of the linear dependence of $\ln t_{cr}$ on H occurs at H_α. The value of H_α decreases with increasing t_w. Above H_α the data of δM ($= M_{\rm TRM} - M_{\rm FC} + M_{\rm ZFC}$) vs. H greatly deviates from zero, where $M_{\rm TRM}$ is the thermal remnant magnetization. This result suggests that the crossover from the quasi equilibrium to the nonequibrium regime occurs at H_α, leading to the violation of FDT.

According to Takayama [8], the H dependence of t_{cr} under the H-shift aging process is governed by three lengths, $L_T(t_{cr}, H)$, $R_T(t_w)$, and the crossover length L_H [1] given by

$$L_H/L_0 \approx (H/\Upsilon_H)^{-1/\delta}, \tag{7}$$

where $\delta = (d/2 - \theta)$ and Υ_H is the magnetic field corresponding to a wall stiffness Υ (a typical energy setting the scale of free energy barriers between conformations). The scaling relation is predicted to exist between the normalized lengths $y = L_T(t_{cr}, H = 0)/L_H$ and $x = R_T(t_w)/L_H$: $y = x - c_H x^{1+\delta}$ with $c_H = 0.15$ for $x < 1$. For $x \ll 1$ corresponding to the case of low H and short t_w, $y = x$, implying that $t_{cr} = t_w$. For $x > 0.2$ corresponding to large H and long t_w, the curve $y(x)$ deviates below the line $y = x$, indicating that t_{cr} is shorter than t_w. From this scaling relation, t_{cr} can be obtained as

$$t_{cr} = t_w \left[1 - c_H (H/\Upsilon_H)(t_w/t_0)^{\delta/z(T)}\right]^{z(T)}. \tag{8}$$

The following features of t_{cr} vs. H are derived from equation (8). (i) The time t_{cr} is not simply proportional to t_w. (ii) In the limit of $H \approx 0$, $\ln t_{cr}$ is linearly dependent on H:

$$\ln(t_{cr}/t_w) = -\alpha_H H,$$

with

$$\alpha_H = z(T)(c_H/\Upsilon_H)(t_w/t_0)^{\delta/z(T)}.$$

The slope α_H increases with increasing t_w. (iii) The T dependence of t_{cr} comes from the exponent $z(T)$. The slope α_H increases with increasing T below T_g mainly because of the factor $(t_w/t_0)^{\delta/z(T)}$.

We find that our results of Figure 8a is consistent with the above predictions. The slope ($\alpha_H = 0.0505 \pm 0.0003$ /Oe) for $t_w = 3.0 \times 10^4$ s is larger than that

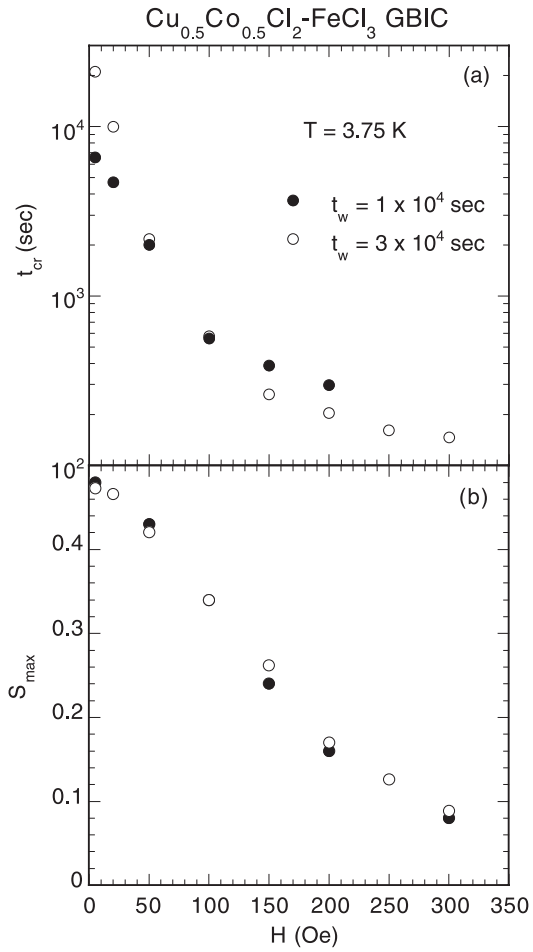

Fig. 8. H dependence of (a) t_{cr} and (b) S_{max} for $t_w = 1.0 \times 10^4$ and 3.0×10^4 s, which is obtained from Figure 7.

($\alpha_H = 0.0262 \pm 0.0005$ /Oe) for $t_w = 1.0 \times 10^4$ s. If we assume that $\delta = 1.37$, $1/z(T) = bT/T_g$, $T_g = 3.92$ K, $b = 0.16$, and $t_0 = \tau^* = 5.29 \times 10^{-6}$ s [26], then the value of Υ_H can be estimated as $\Upsilon_H = 2.15$ kOe for $t_w = 3.0 \times 10^4$ s and $\Upsilon_H = 3.30$ kOe for $t_w = 1.0 \times 10^4$ s. Our numerical calculation of α_H for $3\ {\rm K} \le T \le T_g$ predicts that the slope α_H increases with increasing T below T_g: $\alpha_H = 0.036$ at $T = 3.4$ K and $\alpha_H = 0.044$ at $T = 3.6$ K for $t_w = 3.0 \times 10^4$ s. Although the measurement on α_H vs. T has not been carried out in the present system, this prediction is consistent with the result reported by Zotev et al. [22] in Cu (1.5 at.% Mn) as the increase of α_H vs. T with increasing T for $0.7 < T/T_g < 0.85$.

4.4 S(t) under the T-shift

We have measured the t dependence of $\chi_{\rm ZFC}$ under the T-shift from the initial temperature T_i to the final temperature T_f ($= 3.75$ K $= 0.957 T_g$), where $T_i = 3$, 3.2 3.4, 3.5, 3.6, and 3.9 K. The measurement was carried out after the ZFC aging protocol: quenching of the system from 50 K to T_i, and isothermal aging at $T = T_i$ and $H = 0$ for t_w

($= 3.0 \times 10^3$ and 3×10^4 s). The origin of time ($t = 0$) is a time just after T was shifted from T_i to $T_f = 3.75$ K and subsequently H ($= 5$ Oe) was turned on. Figures 9a and b show the t dependence of S at $T_f = 3.75$ K at various initial temperature T_i. The temperature difference is defined as $\Delta T = T_f - T_i$: the positive T-shift for $\Delta T > 0$ and negative T-shift for $\Delta T < 0$. The relaxation rate $S(t)$ exhibits a peak at $t = t_{cr}$ irrespective of the sign of ΔT. The width of the peak in $S(t)$ for the negative T-shift is much broader than that for the positive T-shift. In Figure 9c we show t_{cr} as a function of ΔT for the positive T-shift for $t_w = 3.0 \times 10^4$ and 3.0×10^3 s. The decrease of t_{cr} with increasing ΔT is observed at low ΔT for both $t_w = 3.0 \times 10^4$ and 3.0×10^3 s. The value of t_{cr} becomes independent of ΔT at large ΔT. For the negative T-shift, on the other hand, the value of t_{cr} for $\Delta T = -0.15$ K ($T_i = 3.9$ K) is larger than that for $\Delta T = 0$ K ($T_i = 3.75$ K) for both $t_w = 3.0 \times 10^4$ and 3.0×10^3 s. Similar behaviors of t_{cr} vs. ΔT for the positive T-shift have been reported by Granberg et al. [Cu (10 at.% Mn)] [13], Djurberg et al. [Cu (13.5 at.% Mn)] [14], and Jonsson et al. [Ag (11 at.% Mn)] [16].

The temperature chaos scenario postulates that the SG equilibrium configurations at different temperatures at T_f and T_i are strongly correlated only up to the overlap-length $L_{\Delta T}$, beyond which these correlations decay to zero. From the droplet theory, the overlap length $L_{\Delta T}$ is described by [1,2]

$$L_{\Delta T}/L_0 \approx \left(T^{1/2}|\Delta T|/\Upsilon_T^{3/2}\right)^{-1/\zeta}, \qquad (9)$$

where ζ is the chaos exponent ($\zeta = d_s/2 - \theta$), d_s is the fractal dimension of the surface of the droplet, and Υ_T is the temperature corresponding to the wall stiffness Υ. From this scenario a scaling relation is predicted to exist between the normalized lengths $y = [L_{Tf}(t_{cr})/L_{\Delta T}]$ and $x = [R_{T_i}(t_w)/L_{\Delta T}]$: $y = x - c_T x^{1+\zeta}$ with $c_T = 0.25$ and $\zeta = 0.385$ for $x < 0.15$ [21,28]. The cumulative aging corresponds to the relation $y = x$ which is valid in the limit $x \approx 0$ (the small $|\Delta T|$ and short t_w). The large $|\Delta T|$ and long t_w corresponds to large x. For $x > 0.05$, the curve y deviates from the straight line $y = x$, corresponding to a rejuvenation due to the temperature chaos effect [21,28]. The value of t_{cr}/t_0 can be described by

$$t_{cr}/t_0 = (t_w/t_0)^{T_i/T_f} \times \left[1 - c_T p(T_f)|\Delta T|(t_w/t_0)^{\zeta/z(T_i)}\right]^{z(T_f)}, \qquad (10)$$

with $p(T_f) = T_f^{1/2}/\Upsilon_T^{3/2}$. In the limit of $|\Delta T| \approx 0$, $\ln t_{cr}$ is linear to T:

$$\ln(t_{cr}/t_w) = -\alpha_T|\Delta T|,$$

with

$$\alpha_T = z(T_f)c_T p(T_f)(t_w/t_0)^{\zeta/z(T_i)}.$$

In fact, the prediction that α_T increases with increasing t_w is experimentally confirmed from Figure 9c. The curve ($\ln t_{cr}$ vs. ΔT) is linearly dependent on ΔT (> 0) for $\Delta T < \Delta T_\alpha$ with the slope α_T: $\alpha_T = 9.9 \pm 0.4$ and $\Delta T_\alpha = 0.3$ K for $t_w = 3.0 \times 10^4$ s and $\alpha_T = 2.6$ and $\Delta T_\alpha \approx 0.15$ K for $t_w = 3.0 \times 10^3$ s. If we assume that $\zeta = 0.385$, $c_T = 0.25$, $1/z(T_f) = bT_f/T_g$, $b = 0.16$, and $t_0 = \tau^* = 5.29 \times 10^{-6}$ s [26] for $t_w = 3.0 \times 10^4$ s, we have $p(T_f) = 1.62 \pm 0.07$ or $\Upsilon_T = 1.12 \pm 0.03$ K for $t_w = 3.0 \times 10^4$ s.

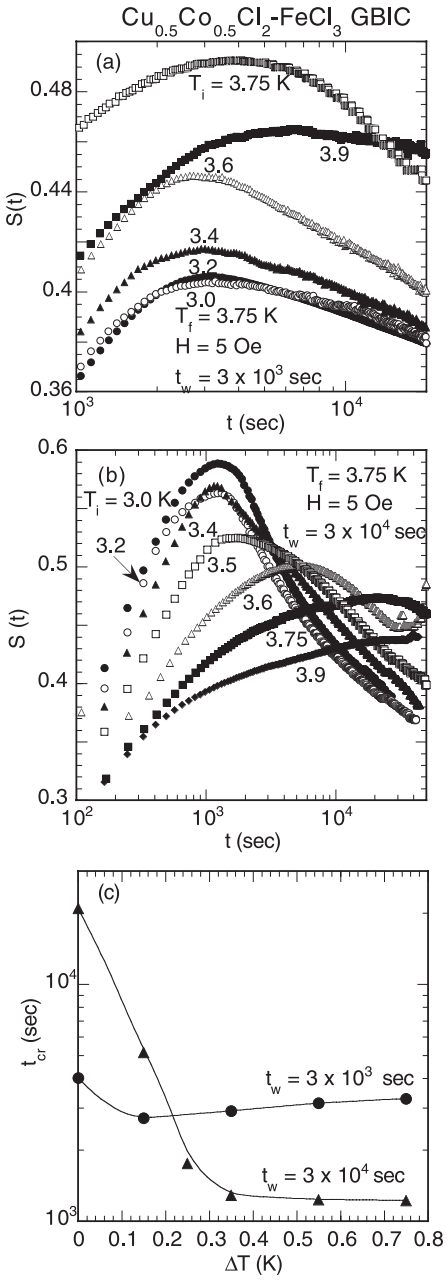

Fig. 9. t dependence of S at $T_f = 3.75$ K under the T shift from T_i to T_f, where $T_i = 3.0$–3.9 K. (a) $t_w = 3.0 \times 10^3$ s. (b) $t_w = 3.0 \times 10^4$ s. The ZFC aging protocol is as follows: quenching of the system from 50 K to T_i, and isothermal aging at $T = T_i$ and $H = 0$ for t_w. The measurement was started at $t = 0$, just after T was shifted from T_i to $T_f = 3.75$ K and subsequently H ($= 5$ Oe) was turned on. (c) t_{cr} vs. ΔT for the case of positive T-shift ($t_w = 3.0 \times 10^3$ and 3.0×10^4 s), where $T_i = T_f - \Delta T$ ($\Delta T > 0$) and $T_f = 3.75$ K. The solid lines are guides to the eye.

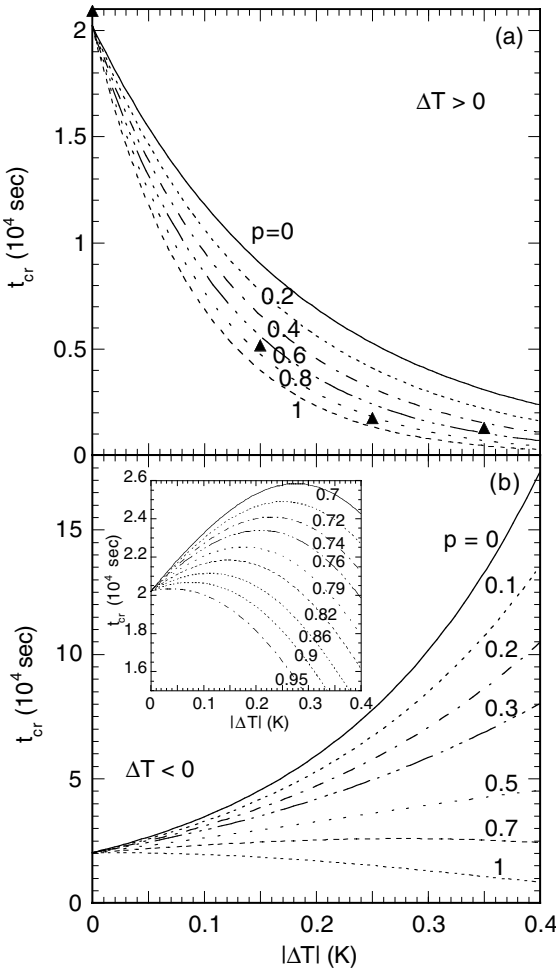

Fig. 10. Numerical calculations of t_{cr} vs. $|\Delta T|$ given by equation (10) for $T_f = 3.75$ K, $T_f = T_i + \Delta T$, and $t_w = t_w(\mathrm{cal}) = 2.04 \times 10^4$ s, where $T_g = 3.92$ K, $b = 0.16$, $\zeta = 0.385$, $c_T = 0.25$, $t_0 = \tau^* = 5.29 \times 10^{-6}$ s, and $0 \leq p(T_f) \leq 1$. (a) The positive T-shift ($\Delta T > 0$). For comparison, our data of t_{cr} vs. ΔT for $t_w = 3.0 \times 10^4$ s are denoted by solid triangles. The value of t_w ($= t_w(\mathrm{cal}) = 2.04 \times 10^4$ s) used in the calculation is different from that used in the experiment [$t_w(\mathrm{exp}) = 3.0 \times 10^4$ s], where $t_w(\mathrm{cal}) = 0.68 t_w(\mathrm{exp})$ (see Fig. 4b). (b) The negative T-shift ($\Delta T < 0$). Although the maximum of $|\Delta T|$ is $T_g - T_f = 0.17$ K in the present system, the value of t_{cr} for the negative T-shift is independent of T_g and is applicable to the other systems with different T_g.

Numerical calculations of equation (10) are carried out as a function of $|\Delta T|$ for $t_w = t_w(\mathrm{cal}) = 2.04 \times 10^4$ s, $T_f = 3.75$ K, $T_i = T - \Delta T$, $\zeta = 0.385$, $t_0 = \tau^* = 5.29 \times 10^{-6}$ s, and $c_T = 0.25$. Note that we use $t_w(\mathrm{cal})$ as t_w instead of $t_w(\mathrm{exp})$ ($= 3.0 \times 10^4$ s) [$t_w(\mathrm{cal}) = 0.68 t_w(\mathrm{exp})$], which leads to the better agreement between our data and calculations at low $|\Delta T|$. In Figures 10a and b we show the results of t_{cr} vs. $|\Delta T|$ for the positive and negative T-shifts, respectively, where $p(T_f)$ is varied as a parameter from 0 to 2.0. For comparison, our data of t_{cr} vs. ΔT with $t_w = 3.0 \times 10^4$ s for the positive T-shift are also plotted in Figure 10a. For the positive T-shift, t_{cr} decreases with increasing ΔT, independent of $p(T_f)$ for $0 \leq p(T_f) \leq 2$. For the negative T-shift, t_{cr} increases with increasing $|\Delta T|$ for $0 \leq p(T_f) < 0.7$. It increases with increasing $|\Delta T|$, showing a peak, and decreases with further increasing $|\Delta T|$ for $0.7 < p(T_f) < 0.92$ (see the inset of Fig. 10b). On the other hand, it decreases with increasing $|\Delta T|$ for $0.92 \leq p(T_f) < 2$. This indicates that t_{cr} decreases with increasing $|\Delta T|$ for both the positive and negative T-shifts for $0.92 \leq p(T_f) < 2$ (the symmetric T-chaos). We find that our data for both the positive and negative T-shifts agree well with the curve with $p(T_f) \approx 0.8$ in Figure 10a, corresponding to $\Upsilon_T = 1.80$ K. This value of Υ_T is on the same order as that derived from the slope α_T.

For Ag (11 at.% Mn) [21], t_{cr} decreases with increasing ΔT for the positive T-shift. For the negative T-shift, however, t_{cr} shifts to the long-t side at $|\Delta T| = 0.1$ K and then t_{cr} decreases with further increasing $|\Delta T|$. Similar behavior has been also observed in Cu (13.5 at.% Mn) [14], where $T_f = 58$ K and $t_w = 3.0 \times 10^3$ s. For the positive T-shift, t_{cr} decreases with increasing ΔT ($0 \leq \Delta T \leq 1.21$ K). For the negative T-shift, t_{cr} increases with increasing $|\Delta T|$ for $0 \leq |\Delta T| \leq 0.6$ K, t_{cr} becomes the longest at $|\Delta T| = 0.6$ K, and t_{cr} decreases with further increasing $|\Delta T|$ for $0.6 \leq |\Delta T| \leq 4.03$ K. These behaviors can be well explained in terms of the scaling relations.

4.5 Memory effect in χ' and χ''

The memory effect in the SG system is defined as follows. When the system is cooled down to a low temperature below T_g, a memory of the spin configurations which is imprinted in the specific cooling sequence, can be recalled when the system is re-heated at a constant heating rate [16,17]. In a single memory experiment, the memory is imprinted at T_1 for t_{w1} during the ZFC aging protocol. In a double memory experiment, the memory is imprinted at T_1 for t_{w1} and at T_2 ($< T_1$) for t_{w2} during the ZFC aging protocol. The dispersion and absorption thus recalled with increasing T are defined as $\chi'_{mem}(\omega, T)$ and $\chi''_{mem}(\omega, T)$, respectively. For comparison, the dispersion and absorption as references [$\chi'_{ref}(\omega, T)$ and $\chi''_{ref}(\omega, T)$], are also obtained with increasing T after the system is quenched from a high temperature above T_g to the lowest temperature. Such AC susceptibility data are called as the ZFC reference susceptibilities, where no memory is imprinted. For clarity we define the difference between the aging ZFC and reference ZFC susceptibilities as $\Delta\chi'(\omega, T) = \chi'_{mem}(\omega, T) - \chi'_{ref}(\omega, T)$ and as $\Delta\chi''(\omega, T) = \chi''_{mem}(\omega, T) - \chi''_{ref}(\omega, T)$. Figures 11a and b show the T dependence of $\Delta\chi'$ and $\Delta\chi''$ for the single memory experiment, where $T_1 = 3.75$ K, $f = 0.05$ Hz, and $h = 0.1$ Oe. Two kinds of measurements were carried out, depending on cooling rate during the ZFC aging protocol: (i) the gradual cooling (gradual decrease of T from 20 to 3.75 K at the cooling rate 5.6×10^{-4} K/s, isothermal aging at $T_1 = 3.75$ K for $t_{w1} = 2.27 \times 10^4$ s, and further gradual decrease from 3.75 to 1.9 K at the rate 2.6×10^{-4} K/s), and (ii) the rapid cooling (quenching of the system from 20 to 3.75 K at $H = 0$ at the rate 0.13 K/s, isothermal aging at $T_1 = 3.75$ K for $t_{w1} = 3.6 \times 10^4$ s, and further quenching from 3.75 to 1.9 K at the rate 0.06 K/s).

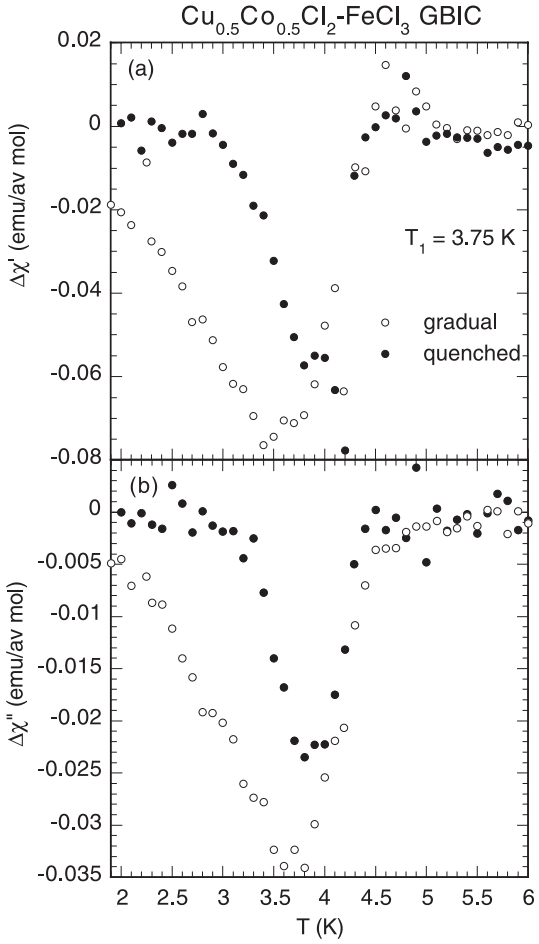

Fig. 11. T dependence of (a) $\Delta\chi'$ and (b) $\Delta\chi''$: single memory experiments (I and II). $f = 0.05$ Hz. $h = 0.1$ Oe. The measurement (I) (denoted as gradual) was carried out after the ZFC aging protocol (I): gradual decrease of T from 20 to 3.75 K, isothermal aging at $T_1 = 3.75$ K for 6.3 hours, and further gradual decrease from 3.75 to 1.9 K. The measurement (II) (denoted as quenched) was carried out after the ZFC aging protocol (II): quenching of the system from 20 to 3.75 K at $H = 0$, isothermal aging at 3.75 K for 10 hours, and further quenching from 3.75 to 1.9 K. Both χ' and χ'' were simultaneously measured with increasing T (aging ZFC curves). $\Delta\chi'$ and $\Delta\chi''$ are the deviations of the aging ZFC curve from the reference ZFC curve measured with increasing T after the standard ZFC aging protocol: quenching from 20 to 1.9 K at $H = 0$.

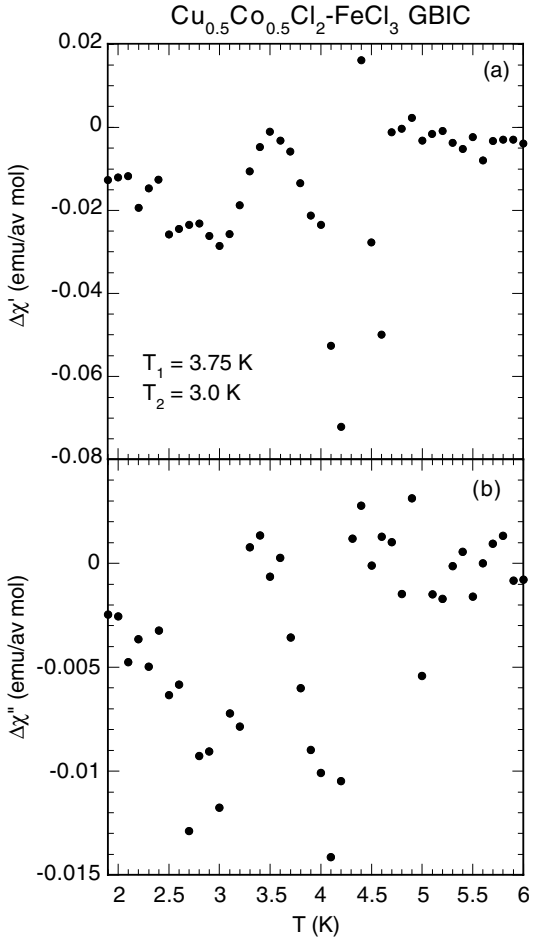

Fig. 12. T dependence of (a) $\Delta\chi'$ and (b) $\Delta\chi''$: double memory experiment. $f = 0.05$ Hz. $h = 0.1$ Oe. $H = 0$. The measurement was carried out after the ZFC aging protocol: quenching of the system from 20 to 3.75 K at $H = 0$, isothermal aging at 3.75 K for 10 hours, quenching from 3.75 to 3.0 K, isothermal aging at 3.0 K for 10 hours, and quenching from 3.0 to 1.9 K. Both χ' and χ'' were si multaneously measured with increasing T (aging ZFC curves). $\Delta\chi'$ and $\Delta\chi''$ are the deviations of the aging ZFC curve from the reference ZFC curve measured with increasing T after the standard ZFC aging protocol: quenching from 20 to 1.9 K at $H = 0$.

Both χ'_{mem} and χ''_{mem} were simultaneously measured with increasing T (aging ZFC curves) from 1.9 to 8 K at the rate 1.7×10^{-4} K/s. The reference ZFC curves (χ'_{ref} and χ''_{ref}) were measured with increasing T from 1.9 to 8 K at the rate 1.7×10^{-4} K/s after the standard ZFC aging protocol: quenching from 20 to 1.9 K at $H = 0$ at the rate 0.15 K/s. The results are as follows. (i) For the case of gradual cooling, $\Delta\chi'$ exhibits negative local minima at 3.4 and 3.75 K, while for the case of rapid cooling, $\Delta\chi'$ exhibits a negative local minimum at 3.75 K. Above 4.3 K, $\Delta\chi'$ is independent of the detail of the ZFC aging protocol. (ii) The absorption $\Delta\chi''$ exhibits a negative local minimum at 3.75 K for both cases of the rapid and gradual cooling. Above 4.1 K, $\Delta\chi''$ is independent of the detail of the ZFC aging protocol. In summary, the equilibration at 3.75 K gives rise to a dip in $\Delta\chi'$ and $\Delta\chi''$, suggesting that the memory of spin configurations which are imprinted during the cooling process, is recalled during the heating. The dip of $\Delta\chi'$ and $\Delta\chi''$ at 3.75 K for the rapid cooling is much narrower than that for the gradual cooling. The reason is that in the case of the gradual cooling the spin configurations at T not equal to 3.75 K are also imprinted during the cooling process. Similar but more pronounced single memory effect has been reported by Jonsson et al. for Ag (11 at.% Mn) [16].

Figures 12a and b show the T dependence of $\Delta\chi'$ and $\Delta\chi''$ for the double memory experiment, where $T_1 = 3.75$ K, $T_2 = 3.0$ K, $f = 0.05$ Hz, and $h = 0.1$ Oe. The measurement was carried out after the ZFC aging protocol

(only in the case of rapid cooling): quenching of the system from 20 to 3.75 K at $H = 0$ at the rate 0.13 K/s, isothermal aging at $T_1 = 3.75$ K for $t_{w1} = 3.6 \times 10^4$ s, quenching from 3.75 to 3.0 K at the rate 0.025 K/s, isothermal aging at $T_2 = 3.0$ K for $t_{w2} = 3.6 \times 10^4$ s, and quenching from 3.0 to 1.9 K at the rate 0.04 K/s. Both χ'_{mem} and χ''_{mem} were simultaneously measured with increasing T (aging ZFC curves). $\Delta\chi'$ and $\Delta\chi''$ are the deviations of the aging ZFC curves from the reference ZFC curves. The results are as follows. Both $\Delta\chi'$ and $\Delta\chi''$ show a small dip at $T_2 = 3.0$ K and a large dip at 4.2 K. There is no dip at $T_1 = 3.75$ K. The magnitudes of $\Delta\chi'$ and $\Delta\chi''$ for the double memory effect are smaller than those for the single memory effect. It seems that the spin configurations which are imprinted at $T_1 = 3.75$ K during the cooling process may be partially reinitialized by the spin configurations imprinted at $T_2 = 3.0$ K. Similar (but more pronounced) double memory effect has been reported by Jonsson et al. for Ag (11 at.% Mn) [16]. The condition for the appearance of the dips at T_1 and T_2 ($= T_1 - \Delta T$) is that the overlap distance $L_{\Delta T}$ given by equation (9) with $T = T_2$ is larger than the size $R_{T_1}(t_{w1})$. The spin configurations imprinted at T_1 is partially reinitialized at T_2, when ΔT is larger than the threshold temperature $(\Delta T)_t$ given by

$$(\Delta T)_t = \left(\Upsilon_T^{3/2}/T_1^{1/2}\right)(t_{w1}/t_0)^{-\zeta/z(T_1)}. \qquad (11)$$

When $t_{w1} = 3.6 \times 10^4$ s, $t_0 = \tau^* = 5.29 \times 10^{-6}$ s, and $\zeta = 0.385$, $(\Delta T)_t$ is estimated as $(\Delta T)_t = 0.14\Upsilon_T^{3/2}$. Using the value of Υ_T (≈ 1.12–1.8 K) obtained in Section 4.4, the value of $(\Delta T)_t$ is estimated as $(\Delta T)_t = 0.16$–0.33 K, which is smaller than $\Delta T = 0.75$ K.

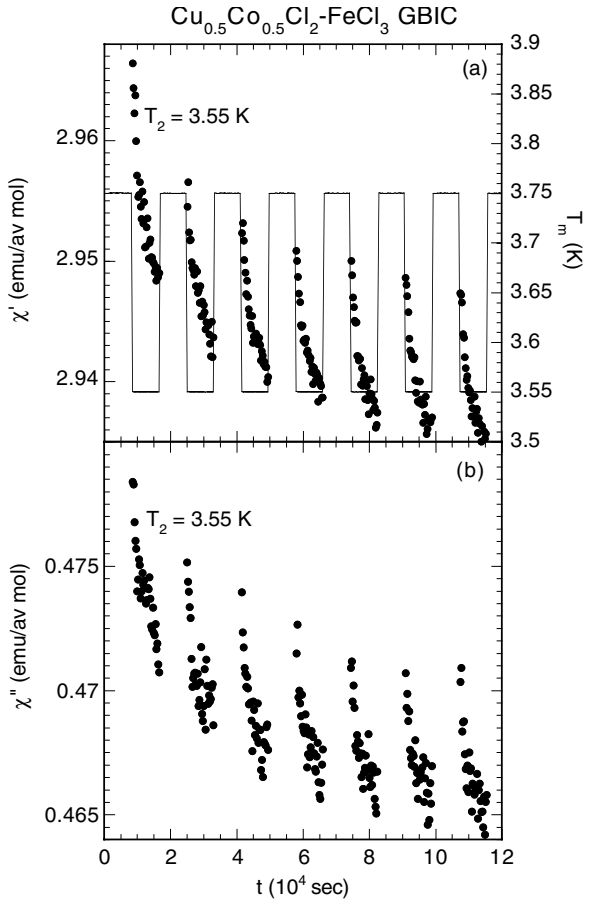

Fig. 13. Relaxation of $\chi'(\omega, t)$ and $\chi''(\omega, t)$ at $T_2 = 3.55$ K during a temperature cycle between $T_1 = 3.75$ K and $T_2 = 3.55$ K. The change of T with t is also shown. $t = 0$ is a time just after the standard ZFC aging protocol: quenching of the system from 50 to 3.75 K at $H = 0$. The data of $\chi''(\omega, t)$ are the same as those presented in reference [26].

4.6 Rejuvenation effect in χ' and χ'' under the T- and H-shifts

The rejuvenation and memory effects in χ' and χ'' under the T-shift are observed in our system. Figures 13a and b show the t dependence of $\chi'(\omega, t)$ and $\chi''(\omega, t)$ at $T_1 = 3.55$ K under the T-shift between $T_1 = 3.75$ K and $T_2 = 3.55$ K, where $f = 0.05$ Hz and $h = 0.1$ Oe. Here the data at $T_1 = 3.75$ K are not shown (see the data of χ'' at $T_1 = 3.75$ K in the previous paper [26]). First our system was quenched from 10 K to $T_1 = 3.75$ K at $H = 0$. The origin of t ($t = 0$) is a time when T becomes T_1. The relaxation of χ' and χ'' was measured as a function of t during a period t_{w1} ($\approx 8.2 \times 10^3$ s). The temperature was then changed to T_2 (the negative T-shift). The relaxation of χ' and χ'' was measured as a function of t for a period t_{w2} ($\approx 8.2 \times 10^3$ s) at T_2. The system was again heated back to T_1 (the positive T-shift). These processes were repeated subsequently. Just after every negative T-shift, both χ' and χ'' do not lie on the reference curves of χ' and χ'' at T_2 obtained when the system is quenched to T_2 directly from 10 K at $t = 0$. The values of χ' and χ'' are larger than the reference curves, indicating the partial reinitialization (rejuvenation) in χ' and χ'' after the negative T-shift. Just after every positive T-shift, however, both χ' and χ'' lie on to the reference curves of χ' and χ'' at T_1 obtained when the system is quenched to T_1 directly from 10 K at $t = 0$, indicating the memory effect in χ' and χ'' after the positive T-shift. Note that the reference curve coincides with a curve where the lowest points for each relaxation in χ' and χ'' are connected as a function of t. The strong rejuvenation effect for the negative T-shift is also predicted from numerical study by Takayama and Hukushima [7] using the MC simulation on the 3D Ising EA SG model. Here we note that the threshold temperature differences under the positive and negative T-shift between T_1 and T_2, $(\Delta T)_+$ and $(\Delta T)_-$, are given by

$$(\Delta T)_+ = \left(\Upsilon_T^{3/2}/T_2^{1/2}\right)(t_{w2}/t_0)^{-\zeta/z(T_2)},$$
$$(\Delta T)_- = \left(\Upsilon_T^{3/2}/T_1^{1/2}\right)(t_{w1}/t_0)^{-\zeta/z(T_1)}, \qquad (12)$$

respectively. When $T_1 = 3.75$ K, $T_2 = 3.55$ K, $t_{w1} = t_{w2} = 8.2 \times 10^3$ s, $t_0 = \tau^* = 5.29 \times 10^{-6}$ s, and $\zeta = 0.385$, we have $(\Delta T)_+ = 0.148\Upsilon_T^{3/2}$ and $(\Delta T)_- = 0.163\Upsilon_T^{3/2}$: $(\Delta T)_+ = 0.18$ K and $(\Delta T)_- = 0.19$ K for $\Upsilon_T = 1.12$ K.

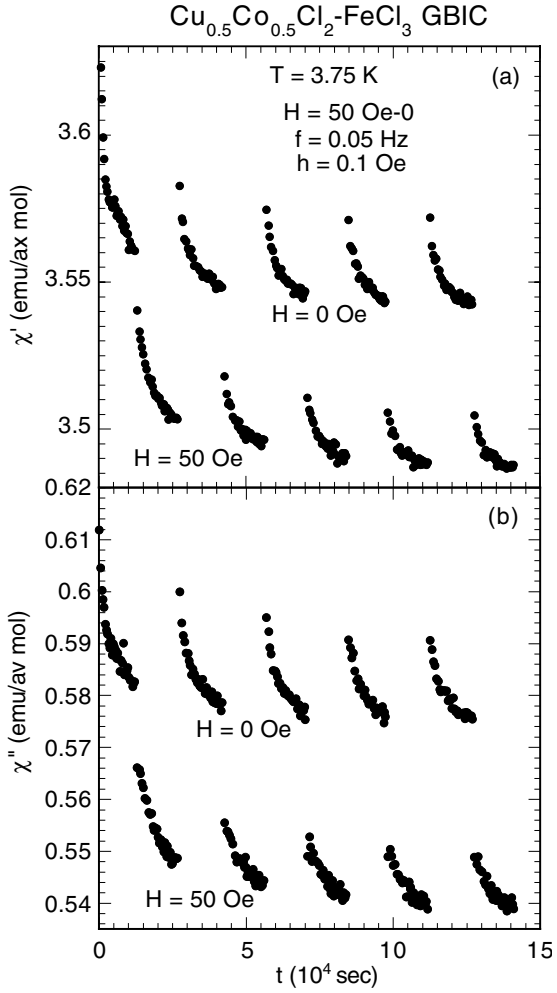

Fig. 14. Relaxation of $\chi'(\omega, t)$ and $\chi''(\omega, t)$ during a magnetic-field cycle between $H = 0$ and 50 Oe. $T = 3.75$ K. $t = 0$ is a time just after the standard ZFC aging protocol: quenching of the system from 50 to 3.75 K at $H = 0$. The data of $\chi''(\omega, t)$ are the same as those presented in reference [26].

Thus the values of $(\Delta T)_+$ and $(\Delta T)_-$ are comparable to the difference $T_1 - T_2 = 0.20$ K.

The rejuvenation effect in χ' and χ'' under the H-shift is also observed in our system. Figures 14a and b show the t dependence of χ' and χ'' at $T = 3.75$ K under the H-shift, where $f = 0.05$ Hz and $h = 0.1$ Oe. After the ZFC aging protocol (quenching from a high temperature above T_g to a temperature T (= 3.75 K)), χ' and χ'' at $H = 0$ were measured for a period t_{w1} ($\approx 1.3 \times 10^4$ s), where the origin of t ($t = 0$) is a time when T becomes 3.75 K. The field is changed from 0 to H (= 50 Oe) at $t = t_{w1}$, After this H-shift, χ' and χ'' were measured for a period t_{w2} ($\approx 1.3 \times 10^4$ s). Subsequently, the field was turned off from H to 0 and the measurements were carried out at $H = 0$ for a period t_{w1}. This process was repeated. We find that both χ' and χ'' undergo drastic jumps under the H-shift (from 0 to 50 Oe) to values higher than the reference curves at $H = 50$ Oe. They also undergo drastic jump under the H-shift (from 50 to 0 Oe) to values higher than the reference curves at $H = 0$. These results suggest that a partial reinitialization (rejuvenation effect) of χ' and χ'' occurs for the H-shifts (0 to 50 Oe and 50 to 0 Oe). Note that the point at $T = 3.75$ K and $H \approx 50$ Oe is located on the de Almeida-Thouless (AT) [30] line in the (H, T) phase diagram [26]. On this AT line, the T-derivative $\mathrm{d}\delta/\mathrm{d}T$ shows a local minimum, where $\delta = \chi_{\mathrm{FC}} - \chi_{\mathrm{ZFC}}$.

When the overlap distance L_H given by equation (7) is smaller than the size $R_T(t_w)$, the spin configuration imprinted at $H = 0$ is partially reinitialized at H ($> H_t$), where the threshold magnetic field is defined as

$$H_t = \Upsilon_H (t_w/t_0)^{-\delta/z(T)}. \tag{13}$$

When $t_w = 3.6 \times 10^4$ s, $t_0 = \tau^* = 5.29 \times 10^{-6}$ s, $\delta = 1.37$, and $T = 3.75$ K, H_t is estimated as $H_t = 8.67 \times 10^{-3} \Upsilon_H$. Using the value of Υ_H (= 2–3 kOe) obtained in Section 4.3, the value of H_t is estimated as 17–25 Oe, which is lower than 50 Oe.

5 Discussion and conclusion

The non-equilibrium nature of the spin dynamics in 3D Ising SG $Cu_{0.5}Co_{0.5}Cl_2$-$FeCl_3$ GBIC has been studied from the t dependence of χ_{ZFC}, χ', and χ'' after specific ZFC protocols including the T-shift (ΔT) and H-shifts. The relaxation rate $S(t)$ shows a peak at t_{cr} ($\approx t_w$), corresponding to a crossover from quasi-equilibrium dynamics to non-equilibrium dynamics. The value of t_{cr} strongly depends on the wait time t_w, T, H, and ΔT. The rejuvenation effects are observed in χ' and χ'' under the negative T-shift and both the positive and negative H-shifts. The spin configurations imprinted under the ZFC aging protocols are recalled on heating the system.

We find that the observed change of t_{cr} under the T-and H-shifts is well explained in terms of the scaling relations where the overlap lengths $L_{\Delta T}$ and L_H play a significant role. Under the T-shift from $T = T_i$ to T_f (= $T_i + \Delta T$), the size of domains are unaffected for sufficiently small $|\Delta T|$, where $L_{\Delta T}$ is larger than $R_{Ti}(t_w)$. Then the relaxation rate $S(t)$ shows a peak at t_{cr} where $L_{T_f}(t)$ is equal to $R_{T_i}(t_w)$. In contrast, the size of domains are affected for sufficiently large $|\Delta T|$. The overlap length $L_{\Delta T}$ becomes lower than $R_{T_i}(t_w)$. Then $S(t)$ has a peak at t_{cr}, where $L_{T_f}(t)$ is equal to $L_{\Delta T}$. Under the H-shift, the size of domains are unaffected during the H shift for sufficiently small H, where the overlap length L_H is larger than $R_T(t_w)$. The value of t_{cr} is dependent on t_w. In contrast, the size of domains are affected during the H shift for sufficiently large H, where L_H becomes lower than $R_T(t_w)$. Then $S(t)$ has a peak at t_{cr}, where $L_T(t) \approx L_H$.

We discuss the scaling relation of the T dependent relaxation rate $S(T, t)$. As pointed out in Section 4.1 $\chi_{\mathrm{ZFC}}(T, t)$ below T_g may be described by a scaling function

$$\chi_{\mathrm{ZFC}}(T, t) = G(x), \tag{14}$$

with $x = L_T(t)/R_T(t_w)$. From the definition, $S(T,t)$ is derived as

$$S(T,t) = \mathrm{d}\chi_{\mathrm{ZFC}}(T,t)/\mathrm{d}\ln t = (1/z(T))H(x), \qquad (15)$$

with $H(x) = x(\mathrm{d}G(x)/\mathrm{d}x)$. It follows that $S(t)$ is described by a scaling function $H(x)$ except for the factor $1/z(T)$. When the scaling function $H(x)$ has a peak at $x = a$ (constant), then $S(t)$ has a peak at $t = t_{cr}$, where $x = L_T(t)/R_T(t_w) = a$. Then t_{cr} is simply described as

$$\ln(t_{cr}/t_w) = (T_g/bT)\ln a. \qquad (16)$$

When a is larger than 1, $\ln(t_{cr}/t_w)$ increases with decreasing T. In fact, the least squares fit of the data of $\ln(t_{cr}/t_w)$ vs. t with $t_w = 2.0 \times 10^3$ s in Figure 3a ($H = 1$ Oe) to equation (16) yields to $(T_g/b)\ln a = 37.1 \pm 1.9$. Since $T_g = 3.92$ K and $b = 0.16$, we have $a = 4.5 \pm 0.4$. It is predicted from equation (15) that S_{max} increases with increasing T for $T < T_g$ since S_{max} is linearly dependent on the factor $1/z(T)$ $(= bT/T_g)$. Experimentally, as shown in Figure 3b with $t_w = 2.0 \times 10^3$ s, the peak height S_{max} strongly depends on T. The peak height S_{max} exhibits a broad peak around 3.6–3.8 K, just below T_g. The linear increase of S_{max} with increasing T below T_g is considered to be due to the factor $1/z(T)$. The decrease of S_{max} with increasing T above T_g, however, cannot be explained in terms of the above model because the scaling relation is valid only for $T < T_g$. In Section 4.1 we show that $S(t)/S_{max}$ at $T = 3.75$ K and $H = 5$ Oe obeys a t/t_w-scaling law for long t_w ($5.0 \times 10^3 \le t \le 1.5 \times 10^4$ s) and $0 \le t \le 6.0 \times 10^4$ s (see Fig. 4c): $S(t)/S_{max}$ is well described by a scaling function $F(t/t_w)$ which has a peak at $t_{cr}/t_w \approx 0.68$. Using equation (16), the value of a is estimated as $a = 1.11$, indicating that the constant a at $H = 5$ Oe is different from that at $H = 1$ Oe.

Finally we consider the cause of the complicated behavior of $S(t)$ at $T = 3.75$ K for $0 \le t_w \le 750$ s. One of the cause is the way how T approaches 3.75 K during the ZFC aging protocol. The temperature drops rapidly to ≈3.50 K and slowly approaches 3.75 ± 0.01 K from the below (usually) within 230 s. The experiment of $S(t)$ under the T shift (see Sect. 4.4) suggests that the initial undercool is not so important because of the temperature difference larger than the threshould temperature difference $(\Delta T)_t$ [23]. However, the subsequent approach of T to 3.75 K for a wait time t_{w0} (≤ 230 s) may play a significant role in the aging behavior after $t = 0$ at $T_m = 3.75$ K. The threshold temperature difference $(\Delta T)_t$ is estimated as

$$(\Delta T)_t = \left(\Upsilon_T^{3/2} / \left[(T_m - (\Delta T)_t)^{1/2}\right]\right) \times (t_{w0}/t_0)^{-\zeta/z(T_m-(\Delta T)_t)}, \qquad (17)$$

from the condition that $L_{\Delta T} = R_{T-\Delta T}(t_{w0})$. When $t_0 = \tau^* = 5.29 \times 10^{-6}$ s, $\zeta = 0.385$, and $t_{w0} = 230$ s, $(\Delta T)_t$ is estimated as $(\Delta T)_t = 0.24$ K for $\Upsilon_T = 1.12$ K and 0.56 K for $\Upsilon_T = 1.80$ K. This suggests that the spin configuration at $T_m = 3.75$ K after $t = 0$ is affected by that imprinted at $T_m - \Delta T$ at the wait time t_{w0}. Note that the value of t_{cr} at $T_m - \Delta T$ is larger than that at T_m for the same t_w (see Fig. 3a). The appearance of two peaks in S vs. t at $0 \le t_w \le 200$ s may be associated with two domains generated for the wait time t_{w0} at $T_m - \Delta T$ and for t_w at T_m.

In conclusion, we have undertaken an extensive study on the t dependence of the relaxation rate $S(t)$ mainly below T_g under the various conditions including the T- and H-shifts. The t dependence of S is well explained in terms of the scaling relation. The peak of $S(t)$ occurs when the mean SG domain size $L_T(t)$ coincides with $R_T(t_w)$, where t_w is the wait time. Our results indicate that the aging, memory and rejuvenation phenomena observed in our system are very similar to those in conventional spin glass systems.

We would like to thank H. Suematsu for providing us with single crystal kish graphite and T. Shima and B. Olson for their assistance in sample preparation and X-ray characterization. Early work, in particular for the sample preparation, was supported by NSF DMR 9201656.

References

1. D.S. Fisher, D.A. Huse, Phys. Rev. B **38**, 373 (1988); D.S. Fisher, D.A. Huse, Phys. Rev. B **38**, 386 (1988)
2. T. Komori, H. Yoshino, H. Takayama, J. Phys. Soc. Jpn **68**, 3387 (1999); T. Komori, H. Yoshino, H. Takayama, J. Phys. Soc. Jpn **69**, 1192 (2000); T. Komori, H. Yoshino, H. Takayama, J. Phys. Soc. Jpn **69**, Suppl. A, 335 (2000)
3. H. Yoshino, A. Lemaître, J.-P. Bouchaud, Eur. Phys. J. B **20**, 367 (2001)
4. M. Picco, F. Ricci-Tersenghi, F. Ritort, Eur. Phys. J. B **21**, 211 (2001)
5. L.W. Bernardi, H. Yoshino, K. Hukushima, H. Takayama, A. Tobo, A. Ito, Phys. Rev. Lett. **86**, 720 (2001)
6. H. Yoshino, K. Hukushima, H. Takayama, Phys. Rev. B **66**, 064431 (2002)
7. H. Takayama, K. Hukushima, J. Phys. Soc. Jpn **71**, 3003 (2002)
8. H. Takayama, J. Mag. Mag. Mater. **272-276**, 256 (2004)
9. L. Berthier, J.-P. Bouchaud, Phys. Rev. Lett. **90**, 059701 (2003)
10. L. Lundgren, in *Relaxation in Complex Systems and Related Topics*, edited by I.A. Campbell, C. Giovannella (Plenum Press, New York, 1990), p. 3
11. J. Hammann, M. Ocio, E. Vincent, *in Relaxation in Complex Systems and Related Topics*, edited by I.A. Campbell, C. Giovannella (Plenum Press, New York, 1990), p. 11
12. P. Nordblad, P. Svedlindh, L. Lundgren, L. Sandlund, Phys. Rev. B **33**, 645 (1986)
13. P. Granberg, L. Sandlund, P. Nordblad, P. Svedlindh, L. Lundgren, Phys. Rev. B **38**, 7097 (1988)
14. C. Djurberg, K. Jonason, P. Nordblad, Eur. Phys. J. B **10**, 15 (1999)

15. Y.G. Joh, R. Orbach, G.G. Wood, J. Hammann, E. Vincent, Phys. Rev. Lett. **82**, 438 (1999)
16. T. Jonsson, K. Jonason, P. Jönsson, P. Nordblad, Phys. Rev. B **59**, 8770 (1999)
17. K. Jonason, P. Nordblad, E. Vincent, J. Hammann, J.-P. Bouchaud, Eur. Phys. J. B **13**, 99 (2000)
18. J.-P. Bouchaud, V. Depuis, J. Hammann, E. Vincent, Phys. Rev. B **65**, 024439 (2001)
19. V. Dupuis, E. Vincent, J.-P. Bouchaud, J. Hammann, A. Ito, H. Aruga Katori, Phys. Rev. B **64**, 174204 (2001)
20. P.E. Jönsson, H. Yoshino, P. Nordblad, H. Aruga Katori, A. Ito, Phys. Rev. Lett. **88**, 257204 (2002)
21. P.E. Jönsson, H. Yoshino, P. Nordblad, Phys. Rev. Lett. **89**, 097201 (2002)
22. V.S. Zotev, G.G. Kenning, R. Orbach, Phys. Rev. B **66**, 014412 (2002)
23. V.S. Zotev, G.F. Rodriguez, R. Orbach, E. Vincent, J. Hammann, Phys. Rev. B **67**, 184422 (2003)
24. F. Bert, V. Dupuis, E. Vincent, J. Hammann, J.-P. Bouchaud, Phys. Rev. Lett. **92**, 167203 (2004)
25. G.F. Rodriguez, G.G. Kenning, R. Orbach, Phys. Rev. Lett. **91**, 037203 (2003)
26. I.S. Suzuki, M. Suzuki, Phys. Rev. B **68**, 094424 (2003)
27. G.G. Kenning, G.F. Rodriguez, R. Orbach, `arXiv: cond-mat/0402509` (2004)
28. P.E. Jönsson, H. Yoshino, P. Nordblad, Phys. Rev. Lett. **90**, 059702 (2003)
29. J.-O. Andersson, J. Mattsson, P. Svedlindh, Phys. Rev. B **46**, 8297 (1992)
30. J.R.L. de Almeida, D.J. Thouless, J. Phys. A **11**, 983 (1978)